Complete All-Optical Silica Fiber Isolator via Stimulated Brillouin Scattering

Xinpeng Huang and Shanhui Fan, *Fellow, IEEE, Fellow, OSA*

***Abstract*—This study demonstrates the theoretical operation of an all-optical silica fiber isolator using stimulated Brillouin scattering. Two pump sources that copropagate through a double-mode fiber generate acoustic waves through electrostriction. These acoustic waves then induce unidirectional interband optical transitions between a separate pair of signal sources. With 1 W of total input pump power, complete optical isolation is achieved with a silica rod waveguide of radius 0.67 μm over a length of approximately 12 m, with pumps operating at a wavelength of 1.55 μm and signals at 1.50 μm.**

***Index Terms*—Brillouin scattering, electrostriction, optical fibers, optical isolators.**

I. Introduction

OPTICAL isolators, which allow light propagation in only one direction, are required in optical and photonic applications for suppressing optical backscattering, which in many cases is a major source of interference and noise [1]. Because complete optical isolation requires time-reversal symmetry breaking, isolators have traditionally been constructed with magneto-optical materials [2]. Despite much effort, these materials still present considerable difficulty for either on-chip or in-fiber integration. The lack of CMOS-compatible optical isolators, for example, has been recognized as a major obstacle in integrated photonics [1], [3]. Methods that have been proposed using nonmagnetic materials [4], [5] typically suffer from shortcomings such as modulation sidebands or power-dependent behavior.

Recent work by Yu and Fan [6]–[8] suggests a mechanism to approach the problem of CMOS-compatible optical isolation by inducing interband photonic transitions. Modulating a silicon waveguide with a sinusoidal dielectric perturbation in space and time will, for suitable frequency and wave vector choices, subject light propagating through the device to interband transitions, similar to electron transitions in semiconductors. By appropriately designing the band structure of the waveguide, Yu and Fan have shown that the induced interband transition breaks time-reversal symmetry, converting propagating light of a frequency ω_1 to a different frequency ω_2 in one direction but not the other. The mechanism is illustrated in Fig. 1(a). It has been shown that such a mechanism can be used to construct an optical circulator that completely reproduces the functionality of a magneto-optical circulator, but without the use of magnetic materials [7].

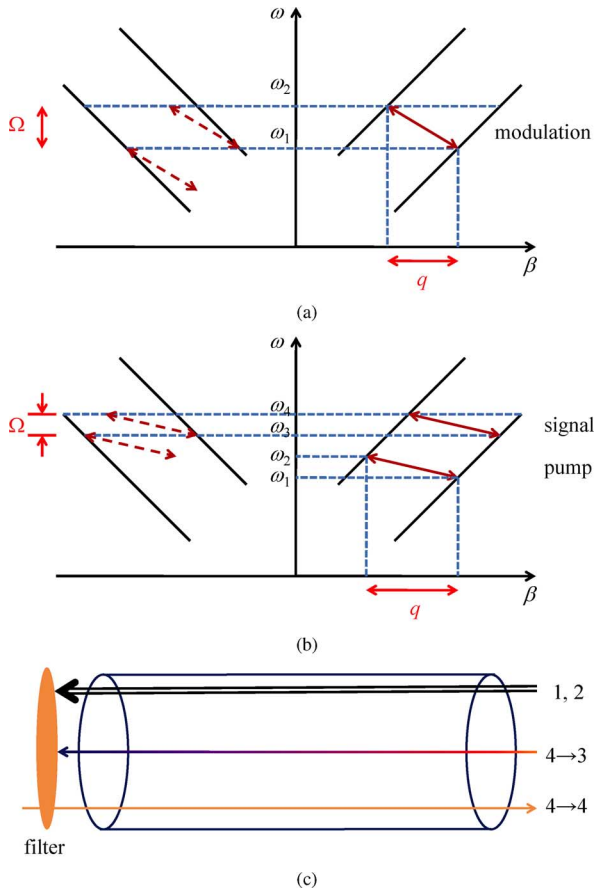

Fig. 1. Optical isolation. (a) Band diagram of time-reversal symmetry breaking through interband transitions induced via direct modulation (dielectric modulation in [6]). (b) Band diagram of the proposed isolator structure. Phonons are electrostrictively generated from two pump sources at ω_1 and ω_2 and are used to induce interband transitions between two signal sources at ω_3 and ω_4. Solid black lines indicate bands, solid red arrows represent allowed transitions, and dashed red arrows represent forbidden transitions due to phase mismatch. Band diagrams are for purely illustrative purposes and are not to scale, nor do they represent any particular structure. Note that transitions are only allowed in one direction, thus permitting optical isolation. (c) One possible realization. Modes are numbered as in (b).

In this paper, we build upon the principles of [6]–[8] to present an all-optical implementation of an isolator that uses photon–phonon interactions to induce nonreciprocal interband transitions in a silica fiber. All materials, including silicon and silica, will strain and deform in response to an electric field gradient traveling through the material. This property, known as

Manuscript received January 31, 2011; revised April 26, 2011; accepted May 23, 2011. Date of publication June 07, 2011; date of current version July 22, 2011.

X. Huang is with the Geballe Laboratory of Advanced Materials, Stanford University, Stanford, CA 94305 USA (e-mail: xph@stanford.edu).

S. Fan is with the Ginzton Laboratory, Department of Electrical Engineering, Stanford University, Stanford, CA 94305 USA (e-mail: shanhui@stanford.edu).

Color versions of one or more of the figures in this paper are available online at http://ieeexplore.ieee.org.

Digital Object Identifier 10.1109/JLT.2011.2158886

electrostriction, is the mechanism behind stimulated Brillouin scattering (SBS), whereby a photon can change its frequency and momentum through a scattering process that releases a phonon [9]. Here, we show that one can use photon–phonon scattering to accomplish the optical isolation effect as first considered by Yu and Fan.

II. Basic Operation

The basic operating principle of the device is shown in Fig. 1. Two optical sources at (β_1, ω_1) and (β_2, ω_2) act as the pump sources, generating phonons of frequency Ω and wave vector q via electrostriction as they copropagate through a waveguide. These phonons are then used to induce interband transitions between two separate signal sources at (β_3, ω_3) and (β_4, ω_4). We note that we use a process involving *copropagating* waves, which is different from the traditional SBS process where optical waves are counterpropagating. In order for the phonons to be generated and for interband transitions to occur, the following relations must be satisfied to conserve energy and momentum:

$$q = \beta_2 - \beta_1 = \beta_4 - \beta_3 \tag{1}$$

$$\Omega = \omega_2 - \omega_1 = \omega_4 - \omega_3. \tag{2}$$

Assume without loss of generality that we begin with an incident signal at (β_4, ω_4), with no input at ω_3. In one direction, the signal photon will have its frequency oscillating between ω_4 and ω_3. The signal photons traveling in the other direction will propagate unaltered due to the nonzero momentum q of the phonons, as is apparent from Fig. 1(b). Thus, the process is nonreciprocal. A modal filter can then be added in order to complete the isolator. A possible implementation is depicted in Fig. 1(c).

III. Theory

We now examine in detail the propagation and interaction of optical and acoustic waves in a waveguide. In order to develop a complete theory of the photon–phonon interaction, we first describe the generation of phonons via electrostriction, which is governed by an acoustic wave equation. We then use this result to calculate the evolution of the pumps, and finally examine the nonreciprocity in signal propagation.

A. Optical Modes

We first take a moment to define precisely the quantities we use to describe the optical modes. There are four optical modes involved in the process, and each mode has a transverse electric field $\mathbf{E}_k$, which can be written as

$$\mathbf{E}_k(x, y, z, t) = \mathbf{e}_k(x, y) a_k(z, t) e^{i(\beta_k z - \omega_k t)} + \text{c.c.} \tag{3}$$

for $k = 1, 2, 3,$ or 4. $\mathbf{e}_k(x, y)$ is the transverse electric field mode profile, a_k is the modal amplitude, and c.c. denotes complex conjugate. The corresponding transverse magnetic field is

$$\mathbf{H}_k(x, y, z, t) = \mathbf{h}_k(x, y) a_k(z, t) e^{i(\beta_k z - \omega_k t)} + \text{c.c.} \tag{4}$$

where $\mathbf{h}_k(x, y)$ is the transverse magnetic field profile. The $k = 1$ and $k = 2$ indexes refer, respectively, to the lower and upper pump sources, and the $k = 3$ and $k = 4$ indexes refer, respectively, to the lower and upper signal sources, as depicted in Fig. 1(b).

The total power carried by a mode is

$$P = (1/2)\Re\{\int (\tilde{\mathbf{E}} \times \tilde{\mathbf{H}}^*) \cdot \hat{\mathbf{z}} \, \mathrm{d}x \, \mathrm{d}y\}$$

[10], where $\tilde{\mathbf{E}}$ and $\tilde{\mathbf{H}}$ are the complex phasor representations of $\mathbf{E}$ and $\mathbf{H}$. In our notation, $\mathbf{E} = \Re\{\tilde{\mathbf{E}} e^{i(\beta z - \omega t)}\} = 2\Re\{\mathbf{e} a e^{i(\beta z - \omega t)}\}$, so we can write

$$P_k = 2|a_k|^2 \int (\mathbf{e}_k \times \mathbf{h}_k) \cdot \hat{\mathbf{z}} \, \mathrm{d}x \, \mathrm{d}y. \tag{5}$$

If we choose the transverse field normalization such that

$$\int |\mathbf{e}_k|^2 \, \mathrm{d}x \, \mathrm{d}y \equiv 1 \tag{6}$$

then we can rewrite (5) in a matter similar to that in [11] as

$$P_k = 2 n_k \varepsilon_0 c s_k |a_k|^2 \tag{7}$$

where $n_k = c\beta_k/\omega_k$ is the effective refractive index, ε_0 is the free-space permittivity, c is the speed of light in vacuum, and

$$s_k = \frac{\int (\mathbf{e}_k \times \mathbf{h}_k) \cdot \hat{\mathbf{z}} \, \mathrm{d}x \, \mathrm{d}y}{n_k \varepsilon_0 c} \tag{8}$$

is a dimensionless number for normalization purposes that becomes unity for a plane wave.

B. Acoustic Wave Equation

The SBS process results from the interaction between optical and acoustic waves in a material via electrostriction [9]. The material vibrations, represented by the material density variation from equilibrium ρ, obey the acoustic wave equation

$$\frac{\partial^2 \rho}{\partial t^2} - V_L^2 \left(1 + \Gamma \frac{\partial}{\partial t}\right) \nabla^2 \rho = \nabla \cdot \mathbf{f} = -\frac{1}{2} \varepsilon_0 \gamma_e \nabla^2 |\mathbf{E}|^2 \tag{9}$$

where V_L is the bulk longitudinal velocity of sound in the waveguide material, Γ is the acoustic damping parameter, $\mathbf{f} = -(1/2)\varepsilon_0 \gamma_e \nabla |\mathbf{E}|^2$ is the electrostrictive force per unit volume, and γ_e is the electrostrictive constant [9], [11]. We define ρ as

$$\rho(x, y, z, t) = \rho_\perp(x, y) b(z, t) e^{i(qz - \Omega t)} + \text{c.c.} \tag{10}$$

where $\rho_\perp(x, y)$ denotes the mode profile of the material density variation and b is the longitudinal acoustic amplitude. In a manner analogous to the optical modes, we normalize $\rho_\perp(x, y)$ such that $\int |\rho_\perp|^2 \, \mathrm{d}x \, \mathrm{d}y = 1$. Solving (9) results in the acoustic amplitude b in the presence of incident electromagnetic waves as characterized by their electric fields $\mathbf{E}$.

Because we are solving a waveguide problem, propagating modes must satisfy specific dispersion relations. If we assume no optical source ($\mathbf{E} = 0$) and no damping ($\Gamma = 0$) in (9), then b must be a constant and can be set to unity. Inserting (10)

into (9) under these conditions yields the following eigenvalue equation:

$$\nabla_\perp^2 \rho_\perp(x,y) = \left(q^2 - (\Omega_a/V_L)^2\right) \rho_\perp(x,y) \tag{11}$$

where $\nabla_\perp^2 \equiv \partial/\partial x^2 + \partial(\partial y^2$ and Ω_a is the frequency of the acoustic mode. Ω_a does not, in general, need to equal $\Omega = \omega_2 - \omega_1$ [11]. Solving (11) results in the acoustic mode profile $\rho_\perp$ and its corresponding wave vector q.

We can now revisit (9) and turn the damping and source terms back on. We insert (10) into the left-hand side of (9), and apply the slowly varying envelope approximation on the derivatives of ρ, ignoring all second-order spatial and temporal derivatives, and using (11) where appropriate. We find

$$\frac{\partial^2 \rho}{\partial t^2} = \rho_\perp \left[-2i\Omega \frac{\partial \rho}{\partial t} - \Omega^2 b\right] e^{i(qz-\Omega t)} + \text{c.c.} \tag{12}$$

$$\nabla^2 \rho = \left[-\frac{\Omega_a^2}{V_L^2} b + 2iq\frac{\partial b}{\partial z}\right] \rho_\perp e^{i(qz-\Omega t)} + \text{c.c.} \tag{13}$$

$$\frac{\partial}{\partial t}\nabla^2 \rho = i\Omega \frac{\Omega_a^2}{V_L^2} b \rho_\perp e^{i(qz-\Omega t)} + \text{c.c.} \tag{14}$$

Now we make the important assumption that the signal power is very weak compared to that of the pump. Consequently, the acoustic wave amplitude ρ is unaffected by $\mathbf{e}_3$ and $\mathbf{e}_4$. Therefore, we can write $\mathbf{E} = \mathbf{E}_1 + \mathbf{E}_2$ and

$$\nabla \cdot \mathbf{f} = -\varepsilon_0 \gamma_e \nabla^2 (\mathbf{e}_1^* \cdot \mathbf{e}_2) a_1^* a_2 e^{i(qz-\Omega t)} + \text{c.c.} \tag{15}$$

Because the acoustic wave in our system is generated by two optical modes propagating in the same direction, $2\pi/q$ will generally be much larger than the target operating wavelength of 1.55 μm. Therefore, the longitudinal variation in $|\mathbf{E}|^2$ varies more slowly than the transverse variation and can, therefore, be neglected, as long as the transverse length scale of the waveguide is around 1 μm or less [11].

Inserting (12)–(15) into (9) yields, after some manipulation,

$$2i\Omega \frac{\partial b}{\partial t} + \left(\Omega^2 - \Omega_a^2 + i\Omega\Gamma_\text{B}\right) b + 2iqV_L^2 \frac{\partial b}{\partial z} = \varepsilon_0 \gamma_e Q_{12}'' a_1^* a_2 \tag{16}$$

where we have defined the Brillouin linewidth $\Gamma_\text{B} \equiv \Omega_a^2 \Gamma$ and introduced the quantity Q_{12}'', defined as

$$Q_{12}'' \equiv \langle \nabla^2 (\mathbf{e}_1^* \cdot \mathbf{e}_2), \rho_\perp \rangle. \tag{17}$$

The notation $\langle f(x,y), g(x,y)\rangle \equiv \int f(x,y) \cdot g^*(x,y)\,\mathrm{d}x\,\mathrm{d}y$ is the inner product on the xy-plane.

Equation (16) can be greatly simplified by neglecting the $\partial b/\partial z$ term, since, in general, phonons are very highly damped and can only propagate over a distance on the order of micrometers before being absorbed by the material [9]. We can now solve for the steady-state ($\partial b/\partial t = 0$) phonon amplitude

$$b(z) = \varepsilon_0 \gamma_e Q_{12}'' \frac{a_1^* a_2}{\Omega^2 - \Omega_a^2 + i\Omega\Gamma_\text{B}}. \tag{18}$$

Note that b depends only on the properties of the two pump modes $(\mathbf{e}_1, a_1)$ and $(\mathbf{e}_2, a_2)$. From the present analysis, it is apparent that electrostriction only generates acoustic waves for pump sources that satisfy $\mathbf{e}_1^* \cdot \mathbf{e}_2 \neq 0$, and therefore, the two optical modes must have the same polarization.

C. Optical Pump Wave Equation

The next step is to calculate how the acoustic wave affects the amplitude of the optical waves. We will first look at the two pumps at ω_1 and ω_2. If we express the electric displacement vector $\mathbf{D}$ in terms of a nonlinear polarization $\mathbf{P}^\text{NL}$ caused by the acousto-optic interaction

$$\mathbf{D} = \varepsilon \mathbf{E} + \mathbf{P}^\text{NL} \tag{19}$$

then from Maxwell's equations, we obtain the optical wave equation

$$\nabla \times \nabla \times \mathbf{E} = -\nabla^2 \mathbf{E} + \nabla(\nabla \cdot \mathbf{E}) = -\mu_0 \varepsilon \frac{\partial^2 \mathbf{E}}{\partial t^2} - \mu_0 \frac{\partial^2 \mathbf{P}^\text{NL}}{\partial t^2}. \tag{20}$$

As a reminder, the electric field $\mathbf{E} = \mathbf{E}_1 + \mathbf{E}_2$ in (20) is the total field, where $\mathbf{E}_1$ and $\mathbf{E}_2$ are expressed according to (3) in terms of the product of the mode profiles $\mathbf{e}_{1,2}$ and the envelopes $a_{1,2}$. Because we are dealing with structures where the permittivity contrast may be large ($\Delta\varepsilon/\varepsilon_0 \sim 1$ for silica, ~ 10 for silicon), we will perform our analysis without assuming that $\nabla \cdot \mathbf{E} \approx 0$, which is only valid for weakly guiding structures.

The nonlinear polarization is $\mathbf{P}^\text{NL} = \varepsilon_0 \gamma_e / \rho_0 \rho \mathbf{E}$ [9], where ρ_0 is the equilibrium density of the material. When $\mathbf{P}^\text{NL}$ is expanded in ρ and $\mathbf{E}$, we only keep the phase-matched terms. Only the $a_2 b^*$ term, corresponding to the conversion $\omega_2 - \Omega = \omega_1$, and the $a_1 b$ term, corresponding to the conversion $\omega_1 + \Omega = \omega_2$, along with their complex conjugates, are properly phase matched. We can, therefore, write $\mathbf{P}^\text{NL}$ as the sum of two propagating terms $\mathbf{P}_1^\text{NL} + \mathbf{P}_2^\text{NL}$ that match the wave vectors and frequencies of the two pump modes (β_1, ω_1) and (β_2, ω_2) [11]:

$$\mathbf{P}_1^\text{NL} = \frac{\epsilon_0 \gamma_e}{\rho_0} \rho_\perp \mathbf{e}_2 a_2 b^* e^{i(\beta_1 z - \omega_1 t)} + \text{c.c.} \tag{21}$$

$$\mathbf{P}_2^\text{NL} = \frac{\epsilon_0 \gamma_e}{\rho_0} \rho_\perp \mathbf{e}_1 a_1 b e^{i(\beta_2 z - \omega_2 t)} + \text{c.c.} \tag{22}$$

Taking derivatives of $\mathbf{P}^\text{NL}$ and applying the slowly varying envelope approximation, we find

$$\frac{\partial^2 \mathbf{P}_1^\text{NL}}{\partial t^2} = \frac{\epsilon_0 \gamma_e}{\rho_0} \rho_\perp \mathbf{e}_2 \left(-a_2 b^* \omega_1^2\right) e^{i(\beta_1 z - \omega_1 t)} + \text{c.c.} \tag{23}$$

$$\frac{\partial^2 \mathbf{P}_2^\text{NL}}{\partial t^2} = \frac{\epsilon_0 \gamma_e}{\rho_0} \rho_\perp \mathbf{e}_1 \left(-a_1 b \omega_2^2\right) e^{i(\beta_2 z - \omega_2 t)} + \text{c.c.} \tag{24}$$

We also take derivatives of the electric field $\mathbf{E}$ to find

$$\nabla^2 \mathbf{E}_k = \left[(\nabla^2 \mathbf{e}_k) a + \mathbf{e}_k \left(2i\beta_k \frac{\partial a_k}{\partial z} - \beta_k^2 a_k\right)\right] \times e^{i(\beta_k z - \omega_k t)} + \text{c.c.} \tag{25}$$

$$\nabla(\nabla\cdot\mathbf{E}_k) = \Big[(\hat{\mathbf{z}}(\nabla\cdot\mathbf{e}_k + 2i\beta_k e_{k,z}) + \nabla e_{k,z})\frac{\partial a_k}{\partial z} + (\nabla(\nabla\cdot\mathbf{e}_k) + i\beta_k\nabla e_{k,z} + \hat{\mathbf{z}}\left(i\beta_k\nabla\cdot\mathbf{e}_k - \beta_k^2 e_{k,z}\right)a\Big] \times e^{i(\beta_k z-\omega_k t)} + \text{c.c.} \quad (26)$$

$$\frac{\partial^2\mathbf{E}_k}{\partial t^2} = \mathbf{e}_k\left(-2i\omega_k\frac{\partial a_k}{\partial t} - \omega_k^2 a_k\right)e^{i(\beta_k z-\omega_k t)} + \text{c.c.} \quad (27)$$

If we solve (20) for the sourceless problem $\mathbf{P}^{\mathrm{NL}} = 0$, $a(z,t) = 1$, then we obtain an expression for the optical mode dispersion as follows:

$$\nabla^2\mathbf{e}_k = \left(\beta_k^2 - \mu_0\varepsilon\omega_k^2\right)\mathbf{e}_k + \nabla(\nabla\cdot\mathbf{e}_k) + i\beta_k\nabla e_{k,z} + \hat{\mathbf{z}}\left(i\beta_k\nabla\cdot\mathbf{e} - \beta_k^2 e_{k,z}\right). \quad (28)$$

Plugging (23)–(28) into (20), applying the overlap integral $\int(\cdots)\cdot\mathbf{e}_k\,\mathrm{d}x\,\mathrm{d}y$ on both sides, and using the normalization condition of (6) yield the following coupled equations for a_1 and a_2 [11]:

$$(1-K_1)\frac{\partial a_1}{\partial z} + \frac{1}{v_{g1}}\frac{\partial a_1}{\partial t} = \frac{i\omega_1\gamma_e}{2n_1 c\rho_0}Q_{12}a_2 b^* \quad (29)$$

$$(1-K_2)\frac{\partial a_2}{\partial z} + \frac{1}{v_{g2}}\frac{\partial a_2}{\partial t} = \frac{i\omega_2\gamma_e}{2n_2 c\rho_0}Q_{12}a_1 b \quad (30)$$

where n_k is the effective index of mode k, v_{gk} is the group velocity, and

$$K_k \equiv \int\left(|e_{k,z}|^2 + \frac{1}{2i\beta_k}(e_{k,z}^*(\nabla\cdot\mathbf{e}_k) + \mathbf{e}_k^*\cdot\nabla e_{k,z})\right)\mathrm{d}x\,\mathrm{d}y \quad (31)$$

is a dimensionless constant that is zero for plane waves and increases as the divergence of the electric field becomes less negligible. We have also defined another quantity Q_{12}, given by

$$Q_{12} \equiv \langle\mathbf{e}_1^*\cdot\mathbf{e}_2, \rho_\perp\rangle \quad (32)$$

in order to simplify notation.

D. Optical Signal Wave Equation

Having performed the derivation for the pump sources, we can do almost exactly the same thing for the signal sources. Equations (29) and (30) undergo slight modifications to become

$$(1-K_3)\frac{\partial a_3}{\partial z} + \frac{1}{v_{g3}}\frac{\partial a_3}{\partial t} = \frac{i\omega_3\gamma_e}{2n_3 c\rho_0}Q_{34}a_4 b^* \quad (33)$$

$$(1-K_4)\frac{\partial a_4}{\partial z} + \frac{1}{v_{g4}}\frac{\partial a_4}{\partial t} = \frac{i\omega_4\gamma_e}{2n_4 c\rho_0}Q_{34}a_3 b \quad (34)$$

where

$$Q_{34} \equiv \langle\mathbf{e}_3^*\cdot\mathbf{e}_4, \rho_\perp\rangle. \quad (35)$$

The only difference between (33), (34) and (29), (30) is that the acoustic amplitude b, given by (18), still depends only on a_1 and a_2, and does not depend on a_3 and a_4. Once again, we are assuming that the signal sources are sufficiently weak and hence do not affect the acoustic mode amplitude.

E. Steady-State Equations

To simplify our analysis, we shall only be concerned with steady-state ($\partial a_k/\partial t = \partial b/\partial t = 0$) solutions from now onwards. Here, we summarize the main theoretical results of this section at steady state. The acoustic amplitude depends on the optical pump amplitudes and is given by

$$b(z) = \varepsilon_0\gamma_e Q_{12}''\frac{a_1^* a_2}{\Omega^2 - \Omega_a^2 + i\Omega\Gamma_{\mathrm{B}}}. \quad (36)$$

The pump amplitudes are given by

$$\frac{\mathrm{d}a_1}{\mathrm{d}z} = \frac{i\omega_1\gamma_e}{2n_1 c\rho_0(1-K_1)}Q_{12}a_2 b^* \quad (37)$$

$$\frac{\mathrm{d}a_2}{\mathrm{d}z} = \frac{i\omega_2\gamma_e}{2n_2 c\rho_0(1-K_2)}Q_{12}a_1 b \quad (38)$$

and the signal amplitudes are

$$\frac{\mathrm{d}a_3}{\mathrm{d}z} = \frac{i\omega_3\gamma_e}{2n_3 c\rho_0(1-K_3)}Q_{34}a_4 b^* \quad (39)$$

$$\frac{\mathrm{d}a_4}{\mathrm{d}z} = \frac{i\omega_4\gamma_e}{2n_4 c\rho_0(1-K_4)}Q_{34}a_3 b. \quad (40)$$

Again, field amplitudes can be converted to optical powers if necessary. Using the normalization condition presented in Section III-A, we can express power as

$$P_k = 2n_k\varepsilon_0 c s_k|a_k|^2. \quad (41)$$

IV. Results

A. Analytical Results

In an attempt to gain some intuition about the general behavior of the coupled (36)–(40) and examine the strength of the mode conversion process, we provide a simplified analytical analysis of the optical and acoustic propagation down the structure.

Substituting (36) into (37) and (38), we obtain the final form of the coupled optical amplitude equations [11]

$$\frac{\mathrm{d}a_1}{\mathrm{d}z} = \frac{i\varepsilon_0\omega_1\gamma_e^2 Q_{12}Q_{12}''}{2n_1 c\rho_0(1-K_1)}\frac{|a_2|^2 a_1}{\Omega^2 - \Omega_a^2 - i\Omega\Gamma_{\mathrm{B}}} \quad (42)$$

$$\frac{\mathrm{d}a_2}{\mathrm{d}z} = \frac{i\varepsilon_0\omega_2\gamma_e^2 Q_{12}Q_{12}''}{2n_2 c\rho_0(1-K_2)}\frac{|a_1|^2 a_2}{\Omega^2 - \Omega_a^2 + i\Omega\Gamma_{\mathrm{B}}}. \quad (43)$$

It is now easier to proceed after converting field amplitudes to optical powers using (41). The final form of the coupled power equations becomes

$$\frac{\mathrm{d}P_1}{\mathrm{d}z} = g_1 P_1 P_2 \quad (44)$$

$$\frac{\mathrm{d}P_2}{\mathrm{d}z} = -g_2 P_1 P_2 \quad (45)$$

where the power gain

$$g_k = g_{k0}\frac{(\Gamma_{\mathrm{B}}/2)^2}{(\Omega-\Omega_a)^2 + (\Gamma_{\mathrm{B}}/2)^2} \quad (k=1,2) \quad (46)$$

is Lorentzian with full-width at half-maximum Γ_B and peak power gain

$$g_{10} = \frac{\omega_1 \gamma_e^2 |Q_{12} Q_{12}''|}{2 n_1 n_2 c^2 \rho_0 \Omega_a \Gamma_B s_2 (1 - K_1)} \tag{47}$$

$$g_{20} = \frac{\omega_2 \gamma_e^2 |Q_{12} Q_{12}''|}{2 n_1 n_2 c^2 \rho_0 \Omega_a \Gamma_B s_1 (1 - K_2)}. \tag{48}$$

Note that the quantity $Q_{12}Q_{12}'' < 0$ because Q_{12}'' includes two spatial derivatives, and therefore, the expressions have been adjusted in favor of the positive quantity $|Q_{12}Q_{12}''|$.

Because $\Omega \ll \omega_{1,2}$, the operating frequencies ω_1 and ω_2 are very close, and therefore, the total power $P = P_1 + P_2$ should be approximately conserved. The same argument can be made for modes 3 and 4. Therefore, even though s_k and K_k depend in complicated ways on the fields $\mathbf{e}_k$ and $\mathbf{h}_k$, power conservation requires that

$$s_2(1 - K_1) = s_1(1 - K_2) \equiv \alpha_{12} \tag{49}$$

$$s_4(1 - K_3) = s_3(1 - K_4) \equiv \alpha_{34}. \tag{50}$$

This simplification allows us to use a single pump gain coefficient

$$g_{10} \approx g_{20} \approx g_0. \tag{51}$$

Suppose that at $z = 0$, we supply pump powers $P_1(0) \equiv P_{10}$ and $P_2(0) \equiv P_{20}$. We wish to calculate the evolution of the optical sources when the correct phase-matching conditions exist to generate phonons. Therefore, let us assume zero detuning ($g = g_0$). Because $(\mathrm{d}/\mathrm{d}z)(P_1(z) + P_2(z)) = 0$, we write $P_1(z) + P_2(z) = P_0$, where P_0 is the total pump power, constant in z. We can then recast (44) into

$$\frac{\mathrm{d}P_1}{\mathrm{d}z} = g_0 P_1 (P_0 - P_1). \tag{52}$$

This is an ordinary differential equation that can be solved analytically. If we define a characteristic length $z_0 = (g_0 P_0)^{-1}$, P_1 can be solved to obtain

$$P_1(z) = \frac{P_0}{1 + (P_{20}/P_{10}) e^{-z/z_0}}. \tag{53}$$

A similar procedure for P_2 yields

$$P_2(z) = \frac{P_0}{1 + (P_{10}/P_{20}) e^{+z/z_0}}. \tag{54}$$

We then proceed to solve for the acoustic amplitude b, which depends on a_1 and a_2. The field amplitudes can be obtained by inserting (53) and (54) into (41). Without loss of generality, we choose the phases of a_1 and a_2 such that both are real for all z, and doing so will make b purely imaginary for all z in the absence of detuning. A straightforward calculation allows us to write

$$b(z) = \frac{\gamma_e Q_{12}''}{i \Omega \Gamma_B \sqrt{n_1 n_2} c} \frac{P_0}{\sqrt{2 + 2\cosh(z/z_0 - \ln(P_{20}/P_{10}))}}. \tag{55}$$

The final step is to solve the coupled equations for a_3 and a_4. Inserting (55) into (39) and (40), we can write

$$\frac{\mathrm{d}a_3}{\mathrm{d}z} = g_3 P_0 f(z) a_4 \tag{56}$$

$$\frac{\mathrm{d}a_4}{\mathrm{d}z} = -g_4 P_0 f(z) a_3 \tag{57}$$

where

$$g_k = \frac{\omega_k \gamma_e^2 |Q_{34} Q_{12}''|}{2 n_k \sqrt{n_1 n_2} c^2 \rho_0 \Omega \Gamma_B \alpha_{34}} \qquad (k = 3, 4) \tag{58}$$

and

$$f(z) \equiv \frac{1}{\sqrt{2 + 2\cosh(z/z_0 - \ln(P_{20}/P_{10}))}}. \tag{59}$$

We can perform a change of variables from z to

$$z' \equiv \int_0^z f(z'')\,\mathrm{d}z'' = z_0 \left(\frac{4\cosh(x/2)\tan^{-1}\tanh(x/4)}{\sqrt{2 + 2\cosh(x)}} - \theta_0 \right) \tag{60}$$

where $x \equiv z/z_0 - \ln(P_{20}/P_{10})$, and

$$\theta_0 \equiv -2\tan^{-1}\left(\frac{\sqrt{P_{20}/P_{10}} - 1}{\sqrt{P_{20}/P_{10}} + 1} \right) \tag{61}$$

is an offset to ensure that $z'(z = 0) = 0$. Using the chain rule $\mathrm{d}a_k/\mathrm{d}z = (\mathrm{d}a_k/\mathrm{d}z')(\mathrm{d}z'/\mathrm{d}z)$, we eliminate the z-dependence in (56) and (57), leaving

$$\frac{\mathrm{d}a_3}{\mathrm{d}z'} = g_3 P_0 a_4 \tag{62}$$

$$\frac{\mathrm{d}a_4}{\mathrm{d}z'} = -g_4 P_0 a_3. \tag{63}$$

Assume that at $z = 0$, we supply power $P_4(0) \equiv P_{40}$, with $P_3(0) \equiv P_{30} = 0$. Then, the solutions are

$$a_3 = A\sin(\sqrt{g_3 g_4} P_0 z') \tag{64}$$

$$a_4 = A\cos(\sqrt{g_3 g_4} P_0 z') \tag{65}$$

where A is some constant that matches the initial conditions. We recognize now that a_3 and a_4 obey standard coupled-mode equations with oscillatory solutions as a function of a variable z' that is distorted through a function $f(z)$ due to the presence of a z-dependence on the acoustic amplitude b. These expressions for a_3 and a_4 can be recast in terms of z_0 by noticing that $\sqrt{g_3 g_4}$ is simply equal to g_0 times a multiplicative factor R. We can also write them in terms of power rather than field amplitude:

$$P_3 = P_{40}\sin^2\left(\frac{R}{2}\frac{z'}{z_0}\right) \tag{66}$$

$$P_4 = P_{40}\cos^2\left(\frac{R}{2}\frac{z'}{z_0}\right) \tag{67}$$

where

$$R \equiv \sqrt{\frac{\omega_3 \omega_4}{\omega_1 \omega_2}} \frac{Q_{34}}{Q_{12}} \frac{\alpha_{12}}{\alpha_{34}} \sqrt{\frac{n_1 n_2}{n_3 n_4}} \approx \frac{\omega_3}{\omega_1} \frac{Q_{34}}{Q_{12}} \frac{\alpha_{12}}{\alpha_{34}} \sqrt{\frac{n_1 n_2}{n_3 n_4}}. \tag{68}$$

Examining these results, we first observe that the pumps P_1 and P_2 are monotonic functions of z, with P_1 increasing to approach P_0 and P_2 decreasing to approach zero. The behavior of

the acoustic amplitude b and the signals P_3 and P_4 are slightly more complex. To aid our analysis, we first look at the simpler case of equal input pump powers, with $P_{10} = P_{20}$ and $\ln(P_{20}/P_{10}) = 0$. Equation (55) becomes a monotonically decreasing function of z for $z > 0$. Because the acoustic amplitude b depends on the product of the two pump amplitudes, and since the total power in the two pumps is conserved, b attains its maximum value when the pumps are equal, which in this case is at $z = 0$.

The behavior of the signal amplitudes can be deduced by analyzing the distorted length z', which is given in (60). Because z' is always less than z for positive values of z, the change of variables effects a "stretching" of the purely sinusoidal solutions that arise from standard coupled-mode theory. The physical interpretation is that there are fewer and fewer phonons available, and therefore, conversion between the signal waves becomes slower as the waves propagate down the structure. For $P_{10} = P_{20}$, $\theta_0 = 0$ and (60) reduces to

$$z' = z_0 \frac{4\cosh(x/2)\tan^{-1}\tanh(x/4)}{\sqrt{2+2\cosh(x)}} \tag{69}$$

with $x \equiv z/z_0$. We are interested in the maximum total conversion rate possible, and therefore, it is a good idea to calculate the highest possible value of z' that can be obtained. Because z' is monotonically increasing, its maximum value corresponds to the $z \to \infty$ limit. It just so happens that $f(z)$ maps $z \to \infty$ to $z'/z_0 \to \pi/2$, because $\int_0^\infty f(z)\,\mathrm{d}z = (\pi/2)z_0$.

In order to determine the behavior of P_3 and P_4, we must also look at the factor R defined in (68). For the case where the four optical sources are operated at almost the same frequency, we notice that the numerator and denominator of R are roughly the same. That is, for $\omega_1 \approx \omega_2 \approx \omega_3 \approx \omega_4 \approx \omega$, $R \approx 1$. Hence, from (66), the maximum possible conversion from P_4 to P_3 is 50%, because the argument of the sinusoid, $(R/2)(z'/z_0)$, never exceeds $\pi/4$. To attain higher conversion, R can be increased by decreasing the frequencies of the pumps and increasing the frequencies of the signals. An R value of 2 must be attained before 100% conversion is possible for any length z.

In Section IV-B, we will see that it is not always easy or desirable to alter the value of R too much by tinkering with the operating frequencies. Another way to increase signal conversion is by altering the initial pump ratio P_{20}/P_{10}. By increasing this ratio, we are creating more phonons that can go into signal conversion. Because $P_1(z)$ always increases and $P_2(z)$ always decreases, we can start P_{10} much lower than P_{20}, and until they propagate to a distance where $P_1(z) = P_2(z)$, they will be generating additional phonons that would not have been present had we started with the pump powers equal. The acoustic amplitude b is now offset by the quantity $\ln(P_{20}/P_{10})$ and will reach its maximum value where the pump powers are equal. Due to the additional phonons, the signals $P_3(z)$ and $P_4(z)$ will undergo a stronger transition. To see this, rewrite (66), evaluated in the limit $z \to \infty$, to obtain

$$\begin{aligned} P_3(z \to \infty) &= P_{40}\sin^2\left(\frac{R}{2}\left(\frac{\pi}{2} - \theta_0\right)\right) \\ &= P_{40}\sin^2\left(\frac{R'}{2}\frac{\pi}{2}\right) \end{aligned} \tag{70}$$

where the effective factor

$$R' = R\left(1 - \frac{2\theta_0}{\pi}\right) \tag{71}$$

has been adjusted for initial pump power ratio. The correction factor $(1-2\theta_0/\pi)$ is larger than one, because from (61), $\theta_0 < 0$ as long as $P_{20}/P_{10} > 1$, and increases as this ratio is increased. For example, for $P_{20}/P_{10} = 99$, $\theta_0 = -1.37$ rad, and R is enhanced by a factor of $(1 - 2\theta_0/\pi) = 1.87$. This means that in order to reach $R' = 2$, we only need to adjust R slightly and bring it to a value of $2/1.87 \approx 1.07$.

B. Numerical Results

Up until now, all of the theory and analysis can be applied to any arbitrary waveguide structure. We now apply the results from Sections III and IV-A to a particular structure: a silica optical fiber with cylindrical symmetry. The structure in consideration requires high modal confinement for the first two fundamental modes, and therefore, we will look at solid-core photonic crystal fibers. As a good approximation, the optical and acoustic properties of such fibers at the frequencies of interest are similar to that of a solid silica rod surrounded by air [11]. Therefore, let us consider a silica rod waveguide of radius a surrounded by air. The derivation of the electric field eigenmodes in an optical fiber is a straightforward calculation, and the result may be found in standard textbooks [12]. In order to calculate the optical dispersion relation $\omega(\beta)$, we must solve the following characteristic equation:

$$\begin{aligned} \frac{\beta^2\nu^2}{a^2}\left(\frac{1}{\gamma^2}+\frac{1}{\kappa^2}\right) = \frac{\omega^2}{c^2}&\left(\frac{J_\nu'(\kappa a)}{\kappa J_\nu(\kappa a)} + \frac{K_\nu'(\gamma a)}{\gamma K_\nu(\gamma a)}\right) \\ &\times\left(\frac{\varepsilon}{\varepsilon_0}\frac{J_\nu'(\kappa a)}{\kappa J_\nu(\kappa a)} + \frac{K_\nu'(\gamma a)}{\gamma K_\nu(\gamma a)}\right) \end{aligned} \tag{72}$$

with

$$\kappa = \sqrt{\left(\frac{\omega n}{c}\right)^2 - \beta^2} \tag{73}$$

$$\gamma = \sqrt{\beta^2 - \left(\frac{\omega}{c}\right)^2}. \tag{74}$$

Also, ν is the mode number, J_ν are Bessel functions of the first kind of order ν, and K_ν are modified Bessel functions of the second kind of order ν [12]. In addition, $J_\nu'(\kappa r) = (\mathrm{d}/\mathrm{d}(\kappa r))J_\nu(\kappa r)$ and $K_\nu'(\gamma r) = (\mathrm{d}/\mathrm{d}(\gamma r))K_\nu(\gamma r)$. We seek the lowest two modes with a minimal E_z component because we know from Sections III-C and III-D that the phonon generation and mode conversion processes rely on the transverse components of the field. The fundamental mode of the rod is the HE_{11} mode, with $\nu = 1$, and will correspond to the $k = 1$ and $k = 3$ optical sources. The next mode is the TE_{01} mode, with $\nu = 0$, corresponding to $k = 2$ and $k = 4$ sources.

We also need to solve for the acoustic eigenmodes of our silica rod. The solutions satisfy the scalar wave equation in cylindrical coordinates (r, ϕ, z) with the boundary condition $\rho = 0$ at the silica–air interface [13], [14]. Furthermore, because the acoustic wave is generated electrostrictively through the beating of a TE_{01} mode with no angular dependence and

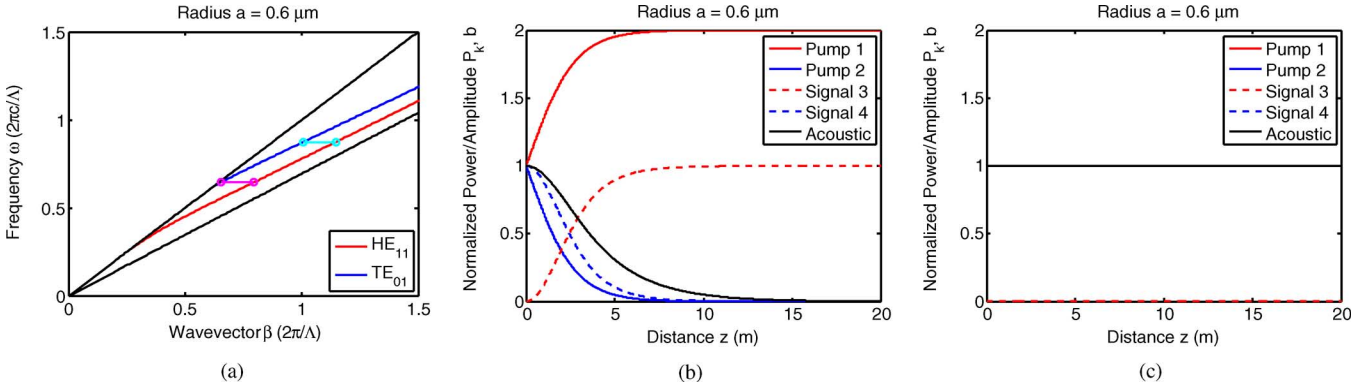

Fig. 2. Simulation results for a cylindrical rod waveguide of radius $a = 0.60\ \mu$m for input pump power ratio $P_{20}/P_{10} = 1$. (a) Band diagram of structure. The lower red curve is the fundamental HE_{11} mode, and the upper blue curve is the TE_{01} mode. The outer black lines are the light lines $\omega = c\beta$ and $\omega = c\beta/n$. Operating points are circled and labeled. β and ω are normalized with respect to $2\pi/\Lambda$ and $2\pi c/\Lambda$, respectively, for $\Lambda = 1\ \mu$m. (b) Pump and signal power, and acoustic wave amplitude, in a rod waveguide as a function of propagation distance z, resulting in unity conversion ($R = 2$). P_1 and P_2 are normalized to $P_0/2$, P_3 and P_4 are normalized to P_{40}, and b is normalized to $b(z = 0)$. (c) Same plot with P_3 and P_4 in the opposite (nonconverting) direction.

an HE_{11} mode with an $e^{i\phi}$ dependence, the resulting acoustic mode must also have an $e^{i\phi}$ dependence for maximum overlap with the optical mode product. Then, we must have

$$\rho_\perp(r,\phi) = C' J_1\left(\frac{r z_1}{a}\right) e^{i\phi} \tag{75}$$

where z_1 is the first zero of J_1. The acoustic dispersion relation then is

$$q_a^2 + \left(\frac{z_1}{a}\right)^2 = \frac{\Omega_a^2}{V_L^2}. \tag{76}$$

To perform the numerical simulation in MATLAB, we first choose a core radius a and calculate the band diagram of the fiber by solving the characteristic equation (72). Next, in order to determine the appropriate frequencies ω_k, we calculate the frequency ω_0 where the two bands are parallel. This is the operating point of highest bandwidth. Starting from $\omega_1 = \omega_3 = \omega_0$, we gradually decrease ω_1 and increase ω_3, while maintaining the phase-matching conditions $\omega_2 - \omega_1 = \omega_4 - \omega_3 = \Omega$ and $\beta_2 - \beta_1 = \beta_4 - \beta_3 = q$, thereby calculating Ω and q for the acoustic waves.

In the first simulation, we start off with equal pump powers, pumping the fiber at $z = 0$ with $P_{10} = P_{20} = 500$ mW. In addition, we provide $P_{40} = 1\ \mu$W and $P_{30} = 0$. As always, we assume that all four optical sources operate at continuous wave and solve only for the steady-state behavior. For each set of valid ω_k, we calculate the optical and acoustic mode profiles, and then perform numerical integration to calculate Q_{12}, Q_{34}, and Q''_{12}. The quantities s_k and K_k are also computed in order to verify (49) and (50). Finally, the optical powers $P_k(z)$ and acoustic amplitude $b(z)$ are calculated by numerical integration of (36)–(40) in z. We use, for silica, $\varepsilon = 2.08\varepsilon_0$, $V_L = 5900$ m/s, $\gamma_e = 1.17$ [11], $\rho_0 = 2200$ kg/m^3, and $\Gamma_\mathrm{B} = 2\pi \times 30$ MHz [15]. In all cases, we find that results obtained from numerical integration agree exactly with analytical results in Section IV-A.

Once the simulation is performed for each set of ω_k values, we select the set for which $R = 2$, which corresponds to the first instance of maximum signal conversion from P_4 to P_3 at $z \to \infty$. The rod radius a can then be adjusted, and the simulation repeated, in order to shift the operating frequencies ω_k. Fig. 2 plots the evolution of the waves, as well as the band diagram with operating points marked, and confirms that there is indeed full conversion from ω_4 to ω_3. We find that for $a = 0.60\ \mu$m, the operating wavelength of the pumps is $\lambda_{1,2} = 2\pi c/\omega_{1,2} \approx 1.55\ \mu$m and that of the signals is $\lambda_{3,4} \approx 1.14\ \mu$m. Unity conversion occurs for a fiber length of $z \sim 8$ m, which is a reasonable length for fiber applications. Although we are lucky enough to attain unity conversion, the signal P_4 is extremely weakly guided, and there is essentially no way to increase R further if we wanted to. In addition, $1.14\ \mu$m is not the most ideal frequency to operate at, because silica is much less lossy at 1.3 or $1.55\ \mu$m. Therefore, for optical communications applications, it is in our interest to keep the frequency ratio $\omega_{3,4}/\omega_{1,2}$ smaller if possible.

In our second simulation, we pump the fiber at $z = 0$ with $P_{10} = 10$ mW and $P_{20} = 990$ mW. The total power P_0 is still 1 W, but now the pump power ratio is $P_{20}/P_{10} = 99$. From Section IV-A, we see that we only need to increase R to 1.07 in order to make the effective ratio $R' = 2$. Taking the exact same steps as before, we plot our results in Fig. 3. Once again, results from numerical integration agree perfectly with theoretical solutions presented in Section IV-A. Unity conversion takes a little longer to occur, at fiber length of $z \sim 12$ m, but the operating frequencies are now much closer together. For a core radius of $a = 0.67\ \mu$m, we have the pumps operating at $\lambda_{1,2} \approx 1.55\ \mu$m and the signals operating at $\lambda_{3,4} \approx 1.50\ \mu$m. This time, because many more phonons (nearly twice as many) are being generated, we only need to increase the gain a little bit in order to achieve $R' = 2$.

Note that in both simulations, running modes 3 and 4 in the reverse direction and assuming nonzero detuning $\Omega \neq \Omega_a$ destroy the conversion process entirely, as can be seen in Figs. 2(c) and 3(c). Thus, we have shown that it is possible to achieve our goal of unity conversion in one direction and zero conversion in the opposite direction using a silica fiber of realistic fiber length and size, and now also suitable frequencies of operation.

C. Discussion

We have numerically calculated that for a silica fiber of length L = 12 m, unidirectional unity conversion can be achieved with

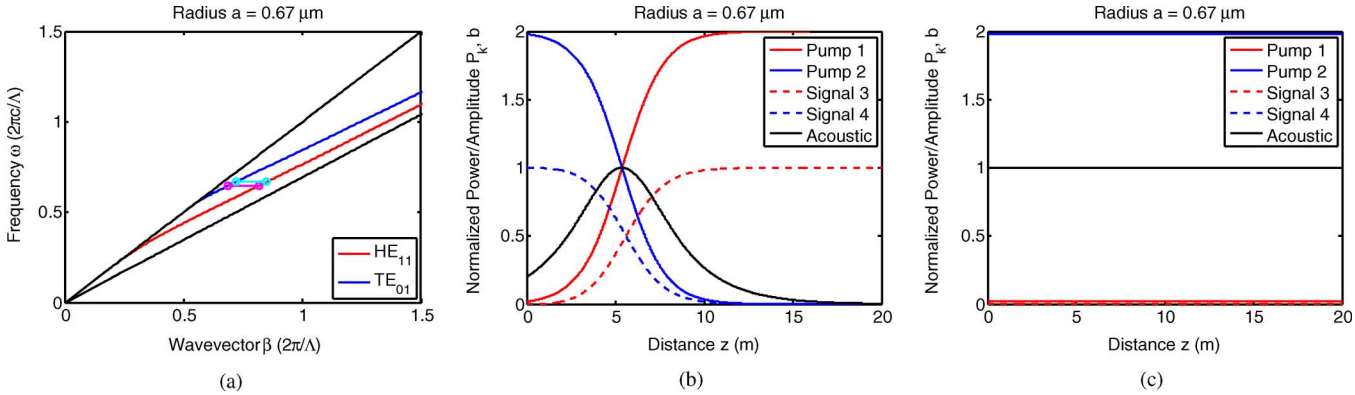

Fig. 3. Simulation results for a cylindrical rod waveguide of radius $a = 0.67\ \mu$m for input pump power ratio $P_{20}/P_{10} = 99$. (a) Band diagram of structure. The lower red curve is the fundamental HE_{11} mode, and the upper blue curve is the TE_{01} mode. The outer black lines are the light lines $\omega = c\beta$ and $\omega = c\beta/n$. Operating points are circled and labeled. β and ω are normalized with respect to $2\pi/\Lambda$ and $2\pi c/\Lambda$, respectively, for $\Lambda = 1\ \mu$m. (b) Pump and signal power, and acoustic wave amplitude, in a rod waveguide as a function of propagation distance z, resulting in unity conversion ($R = 1.07$, $R' = 2$). P_1 and P_2 are normalized to $P_0/2$, P_3 and P_4 are normalized to P_{40}, and b is normalized to $b(z = 0)$. (c) Same plot with P_3 and P_4 in the opposite (nonconverting) direction.

SBS. In this section, we provide a brief discussion of various issues related to the process.

First, to enable complete optical isolation, modal filtering is likely necessary in order to distinguish the optical signals 3 and 4, which are very close in frequency. For this purpose, we note that modal filtering in double-mode fibers has been demonstrated experimentally [16]. Such a modal filter can also be used for selective input into one of the signal modes, which is important for the operation of the isolator.

It should be noted that the bandwidth of the isolator is limited only by the extent to which one can design parallel bands at the signal operating points 3 and 4, and previous work has demonstrated that it is in principle possible to engineer band structures with bandwidth on the order of terahertz [6].

In order to examine the robustness of the isolation effect, we have examined other effects that may potentially impede or overwhelm the proposed photon–phonon interactions. For example, it is well known that spontaneous Brillouin backscattering can occur in a system with just one propagating optical wave, provided the power is high enough. A simple way to model this process is to assume a very weak counterpropagating optical wave generated through the spontaneous process, with a typical power ratio of 10^{-11} to 10^{-12} at the $z = L$ end of the fiber [9], [17]. When we tried to incorporate the effect of spontaneous backscattering on our optical pumps for $L = 12$ m into our numerical calculations, we observed no change in any of the plots in Figs. 2 and 3.

We have also looked into modulation instability, which concerns the stability of the steady-state solutions of the optical modes. Narum *et al.* [18] pointed out that for a long structure with normalized length $2n\Omega L/c \gtrsim 100$, where n is the refractive index, stability tends to improve with unbalanced pumping. For the case considered in Fig. 3, $2n\Omega L/c \approx 4000$ and the pumping ratio is 1:99. Adopting Narum *et al.*'s analysis as a rough guideline, we calculate the quantity $g_0 P_0 L \approx 10$ and note that it is below the threshold value of 15 that is appropriate in the strongly unbalanced pumping case for such a long structure. Thus, we do not believe that modulation instability would disrupt the Brillouin scattering process in our system.

V. Conclusion

In this study, we have demonstrated complete all-optical mode conversion in a medium that does not make use of any magneto-optic effects. We have shown that by appropriately choosing the operating frequencies of the sources and the initial pump power ratio, we can achieve unity conversion between two optical bands in one direction but not the other. By combining this mode conversion with a modal filter, we can enable complete optical isolation in silica. The operation of the device may be further improved by increasing the phonon interaction length within the fiber by coupling pump sources throughout the entire length of the fiber. As it stands, this theoretical and numerical demonstration of optical isolation using SBS is the first step in realizing such a device and holds promise for developing a completely new class of nonreciprocal devices.

References

[1] M. Soljačić and J. D. Joannopoulos, "Enhancement of nonlinear effects using photonic crystals," *Nat. Mater.*, vol. 3, pp. 211–219, Apr. 2004.

[2] L. J. Aplet and J. W. Carson, "A Faraday effect optical isolator," *Appl. Opt.*, vol. 3, no. 4, pp. 544–545, Apr. 1964.

[3] V. R. Almeida, C. A. Barrios, R. R. Panepucci, and M. Lipson, "All-optical control of light on a silicon chip," *Nature*, vol. 431, pp. 1081–1084, Oct. 2004.

[4] K. Gallo, G. Assanto, K. R. Parameswaran, and M. M. Fejer, "All-optical diode in a periodically poled lithium niobate waveguide," *Appl. Phys. Lett.*, vol. 79, no. 3, pp. 314–316, Jul. 2001.

[5] S. K. Ibrahim, S. Bhandare, D. Sandel, H. Zhang, and R. Noé, "Non-magnetic 30 dB integrated optical isolator in III/V material," *Electron. Lett.*, vol. 40, no. 20, pp. 1293–1294, Sep. 2004.

[6] Z. Yu and S. Fan, "Complete optical isolation created by indirect interband photonic transitions," *Nat. Photon.*, vol. 3, pp. 91–94, Feb. 2009.

[7] Z. Yu and S. Fan, "Optical isolation based on nonreciprocal phase shift induced by interband photonic transitions," *Appl. Phys. Lett.*, vol. 94, pp. 171116-1–171116-3, May 2009.

[8] Z. Yu and S. Fan, "Integrated nonmagnetic optical isolators based on photonic transitions (invited paper)," *IEEE J. Sel. Topics Quantum Electron.*, vol. 16, no. 2, pp. 459–466, Mar./Apr. 2010.

[9] R. W. Boyd, *Nonlinear Optics*, 2nd ed. San Diego, CA: Academic, 2003.

[10] U. S. Inan and A. S. Inan, *Engineering Electromagnetics*. Reading, MA: Addison-Wesley, 1999.

[11] M. S. Kang, A. Nazarkin, A. Brenn, and P. S. J. Russell, "Tightly trapped acoustic phonons in photonic crystal fibers as highly nonlinear artificial Raman oscillators," *Nat. Phys.*, vol. 5, pp. 276–280, Apr. 2009.

[12] C. R. Pollock, *Fundamentals of Optoelectronics*. Homewood, IL: Irwin, 1994.

[13] B. A. Auld, *Acoustic Fields and Waves in Solids*, 2nd ed. Huntington, NY: Robert E. Krieger Publishing Co., 1990, vol. I.

[14] E. Peral and A. Yariv, "Degradation of modulation and noise characteristics of semiconductor lasers after propagation in optical fiber due to a phase shift induced by stimulated Brillouin scattering," *IEEE J. Quantum Electron.*, vol. 35, no. 8, pp. 1185–1195, Aug. 1999.

[15] L. Thévenaz, "Fibre distributed sensing for a more secure society," in *Proc. Symp. Photon. Technol. 7th Framework Program*, Oct. 2006, pp. 43–51.

[16] W. V. Sorin, B. Y. Kim, and H. J. Shaw, "Highly selective evanescent modal filter for two-mode optical fibers," *Opt. Lett.*, vol. 11, no. 9, pp. 581–583, Sep. 1986.

[17] R. W. Boyd, K. Rzążewski, and P. Narum, "Noise initiation of stimulated Brillouin scattering," *Phys. Rev. A*, vol. 42, no. 9, pp. 5514–5521, Nov. 1990.

[18] P. Narum, A. L. Gaeta, M. D. Skeldon, and R. W. Boyd, "Instabilities of laser beams counterpropagating through a Brillouin-active medium," *J. Opt. Soc. Amer. B*, vol. 5, no. 3, pp. 623–628, Mar. 1988.

Xinpeng Huang received the S.B. degrees in electrical and electronic engineering and physics from the Massachusetts Institute of Technology, Cambridge, in 2008, and the M.S. degree in electrical engineering from Stanford University, Stanford, in 2010, where he is currently working toward the Ph.D. degree.

Shanhui Fan (F'11) received the Ph.D. degree in theoretical condensed matter physics from the Massachusetts Institute of Technology (MIT), Cambridge, in 1997.

He is currently an Associate Professor of electrical engineering at the Stanford University, Stanford. He was a Research Scientist at the Research Laboratory of Electronics, MIT, prior to his appointment at Stanford. He is the author or coauthor of more than 200 refereed journal articles that were cited 12 000 times, has given more than 150 invited talks, and was granted 39 U.S. patents. His research interests include computational and theoretical studies of solid state and photonic structures and devices, especially photonic crystals, plasmonics, and metamaterials.

Dr. Fan received a National Science Foundation Career Award in 2002, a David and Lucile Packard Fellowship in Science and Engineering in 2003, the National Academy of Sciences Award for Initiative in Research in 2007, and the Adolph Lomb Medal from the Optical Society of America in 2007. He is a Fellow of the American Physical Society, the Optical Society of America, and the International Society for Optical Engineers.